RSC Advances

ROYAL SOCIETY OF CHEMISTRY

www.rsc.org/advances

Journal Name

ARTICLE

Synergetic effect of Cu-Pt bimetallic cocatalyst on $SrTiO_3$ for efficient photocatalytic hydrogen production from water

Received 00th January 20xx,
Accepted 00th January 20xx

DOI: 10.1039/x0xx00000x

www.rsc.org/

Lixia Qin,[a] Guofeng Si,[a] Xiangqing Li,[a] Shi-Zhao Kang*[a]

Herein, a series of novel $SrTiO_3$ (STO) based photocatalysts loaded with Cu-Pt bimetallic co-catalysts have been synthesized through a simple photodeposition process. This photocatalyst of STO/Cu-Pt displayed enhanced photocatalytic activity for hydrogen generation from water in the presence of methanol as a sacrificial reagent. Moreover, the hydrogen generation efficiency over the STO/Cu95-Pt5 photocatalyst was about 2.79 and 1.76 times of STO/Cu100-Pt0 and STO/Cu0-Pt100, respectively. Thus, this Cu-Pt synergetic cocatalyst presents an inexpensive and high efficiency cocatalyst to achieve efficient hydrogen evolution from water.

1 Introduction

As a potential answer to the global energy problem and environmental pollution, the application of hydrogen energy has attracted much attention.[1,2] Since the pioneering report by Fujishima and Honda,[3] a great number of studies are focused on the photocatalytic hydrogen evolution, and it appears to be a promising strategy for clean, low-cost, and environmentally friendly hydrogen production by utilizing solar energy.[4-6] Among various oxide semiconductor photocatalysts, perovskite-type $SrTiO_3$ (STO) has been widely researched for photocatalytic water splitting in that its band structure suits the water redox potential levels to facilitate hydrogen and oxygen formation.[7-10] Studies show that the type and amount of cocatalyst plays a key role in the photocatalytic hydrogen production. It is well known that the loading of Pt as a cocatalyst on STO significantly enhances the hydrogen production efficiency for photocatalytic water reduction in the presence of sacrificial agents. However, Pt is a rare and expensive noble metal. Therefore, alternative based on inexpensive metals and the more optimized multimetal cocatalyst have been actively pursued.

As we all known, these heterogeneous composite catalysts are generally composed of one and more catalytically active components and a functional support, in which the interaction between the catalytic components and the support materials could possibly endow the composite catalysts with much improved catalytic properties, such as significantly enhanced the catalytic activity, chemical stability, and prolonged lifetime.[11] In particular, development in synergistic effect of bimetal will provide access to variety of low-cost and high-performance catalysts for laboratory and industrial applications.[12] The supported bimetallic cocatalyst consisting of inexpensive metal and a spot of noble metal often shows superior catalytic activity, arising from the synergetic catalystic effect of both moieties.[13-16]

In recent years, the supported Cu–M (M mainly referring to Pt, Pd, Ru, Rh, etc) bimetal nanocomposites have attracted considerable attention as highly active, eco-friendly and relatively cheaper catalyst which applied in hydrogenation, oxidation and hydrodechlorination reactions.[17–21] For instance, An Cu-Au bimetal supported on mesoporous TiO_2 have been reported with stable catalytic performance in CO oxidation.[19] Recently, a TiO_2–supported bimetal catalytic system was constructed which show high catalytic activity.[22,23] In particular, the Cu-M (Pt, Pd, Rh, Ru) loading TiO_2 system exhibited high photocatalytic activity towards reducing nitrate.[23] According to our knowledge, the application of STO/Cu-Pt composite photocatalyst with loading CuPt bimetal as cocatalyst for photocatalytic hydrogen has not been reported.

In the present work, we report the synthesis of STO/Cu-Pt photocatalyst for photocatalytic hydrogen production. Results demonstrated that the activity of STO was significantly enhanced when using Cu-Pt bimetallic alloy as cocatalyst. The highest hydrogen production rate over STO/Cu95-Pt5 is up to 369.4 μmol h^{-1}. This unusual photocatalytic activity arises from the positive synergistic catalytic effect between Cu and Pt component in this cocatalyst, which serves as a source of active adsorption sites and photocatalytic reaction centres, respectively.

2. Experimental

2.1 Preparation of the STO nanoparticles loaded with Cu-Pt alloy

The STO nanoparticles were prepared by a polymerized complex method.[24] All the reagents were of analytical grade and used without

[a]School of Chemical and Environmental Engineering, Shanghai Institute of Technology, 100 Haiquan Road, Shanghai 201418, China, E-mail: kangsz@sit.edu.cn.

further purification. Distilled water was used in all experiments. Titanium tetrabutoxide ($Ti[O(CH_2)_3CH_3]_4$, 50 mmol) was dissolved into 150 mL of methanol, then 0.4 mol of anhydrous citric acid (CA) was added to the solution. $SrCO_3$ (50 mmol) and propylene glycol (1.2 mol, Kanto Chemical) were added into the Ti–CA methanol solution. The mixed solution was heated with stirring on a heating plate operating at 353 K until a transparent solution was obtained, then it was heated at 473 K with stirring to promote condensation and esterification. A transparent polyester resin was eventually formed. The obtained resin was subjected to heating in air at 723 K, then at 823 K for 5 h.

The STO nanoparticles loaded with various amounts of Cu-Pt were prepared using a photo-deposition method. A typical experimental procedure was described as followed: 30 mg of the as-prepared STO nanoparticles was dispersed into 60 mL of aqueous methanol solution (50 vol.%). Then, 233 μL of 0.01 $mol \cdot L^{-1}$ $Cu(NO_3)_2$ solution and 63.5 μL of 1 $mg \cdot mL^{-1}$ chloroplatinic acid ($H_2PtCl_6 \cdot 6H_2O$) solution were added into the suspension. After bubbled with highly pure N_2 gas for 30 min to remove the dissolved oxygen gas, the suspension was stirred and irradiated for 30 min by a 500 W high-pressure mercury lamp. In order to describe conveniently, the as-prepared samples are abbreviated, and the abbreviations are listed in Table 1. Similarly, blank STO was alsoprepared following the same procedure as above except that the load of Cu-Pt bimetallic co-catalyst was eliminated.

Table 1 Composition of the STO nanoparticles loaded with Cu-Pt alloy

Sample	Total amount of Cu-Pt alloy loaded (mol%)	Content of Cu in Cu-Pt alloy (mol%)	Content of Pt in Cu-Pt alloy (mol%)
STO/Cu0-Pt0	0	0	0
STO/Cu100-Pt0	1.5	100	0
STO/Cu95-Pt5	1.5	95	5
STO/Cu90-Pt10	1.5	90	10
STO/Cu10-Pt90	1.5	10	90
STO/Cu0-Pt100	1.5	0	100

2.2 Characterizations

The structure and crystalline phase of the samples were characterized with a Rigaku D/max 2550 VB/PC X-ray diffractometer (XRD, Japan) using Cu Kα radiation (λ = 0.154056 nm). The microstructure and morphology of the samples were analyzed on a JEOL, JEM-200CX transmission electron microscope (TEM) with 200 kV accelerating voltage (Japan). The X-ray photoelectron spectrum (XPS) was recorded with a PHI 5000 Versaprobe spectrometer (Japan). The ultraviolet-visible diffuse reflectance absorption spectra (DRS) were recorded on a Shimadzu UV-3101PC UV-vis-NIR spectrophotometer (Japan). The N_2 adsorption and desorption isotherms were measured on a Micromeritics ASAP-2020 nitrogen adsorption apparatus (USA). The photoluminescence spectra (PL) were recorded with a Shimadzu RF-5301PC fluorescence spectrometer (Japan). The energy-dispersive X-ray spectroscopy (EDX) was taken with a JEOL JSM-6360LV electron microscopy (Japan).

2.3 Photocatalytic activity test

The photocatalytic reaction was carried out in a gas-closed system with a quartz reactor. A 500 W high-pressure mercury lamp was used as UV light radiation source. The distance between the lamp and the reactor was maintained to be 20 cm. STO/Cu95-Pt5 was prepared by in situ photo-reduction method and directly used without separation. After bimetallic Cu-Pt alloy was loaded on the STO nanoparticles, the irradiation was kept for hydrogen evolution reaction. The amount of hydrogen evolution was analyzed with a gas chromatograph (GC-7900, molecular sieve 5A, TCD, China) using N_2 as a carrier gas.

3 Results and discussion

The XRD patterns of pure STO (a), STO/Cu100-Pt0 (b), STO/Cu95-Pt5 (c) and STO/Cu0-Pt100 (d) are shown in Fig. 1. It is clearly found that there exist the peaks at 32.4°, 39.9°, 46.4°, 57.8°, 67.8° and 77.2° in the XRD patterns of STO/Cu100-Pt0, STO/Cu95-Pt5 and STO/Cu0-Pt100 (Fig.1 b, c and d), corresponding to the (110), (111), (200), (211), (220) and (310) planes of the cubic STO (JCPDS card no. 35-0734), respectively. In comparison with the pure STO (Fig.1a), all the diffraction peaks of STO in the as-prepared samples do not shift, implying that Cu and Pt atoms are not incorporated into the STO lattice. However, no characteristic diffraction peaks of Cu and Pt species are observed. A possible explanation is the few loading amount of Cu and Pt, or the Cu and Pt particles are too small to give well-defined diffraction peaks.

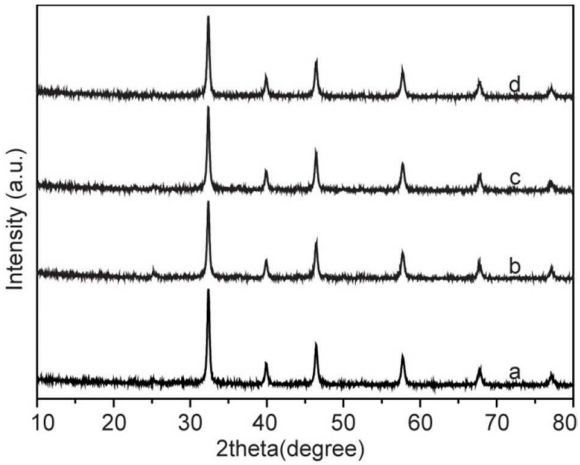

Fig. 1 XRD patterns of pure STO (a), STO/Cu100-Pt0 (b), STO/Cu95-Pt5 (c) and STO/Cu0-Pt100 (d).

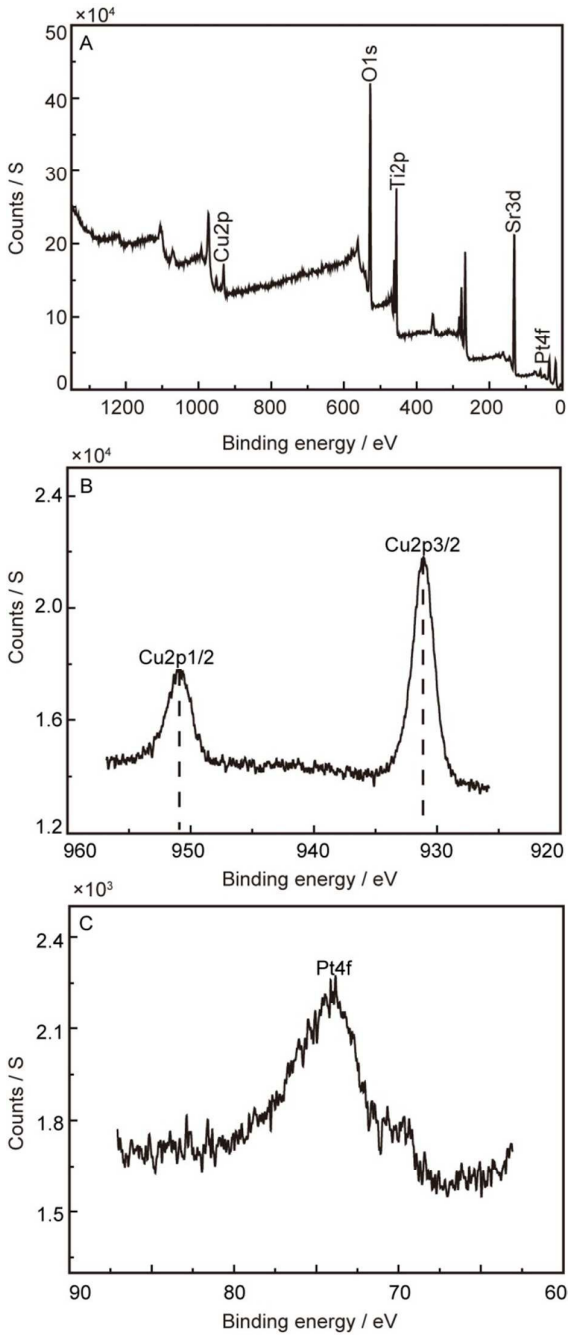

Fig. 2 XPS survey spectrum of STO/Cu95Pt0.5 (A), high-resolution XPS of Cu 2p spectrum (B) and high-resolution XPS of Pt 4f spectrum (C).

In addition, the evidence for the composition of STO/Cu95-Pt5 was obtained by XPS analysis (Fig. 2). The sample was prepared under vacuum for more than 10 h and then purged with highly pure N_2 gas for 30 min to remove the dissolved oxygen gas before irradiation. After photodeposition, obviously, the XPS analysis confirms that there exist elements Sr, Ti, O, Cu and Pt on the surface of STO/Cu95-Pt5 (Fig. 2A). Also, the result of high-resolution XPS spectrum of Cu 2p (Fig. 2B) clearly shows that there exist two peaks at 931.5 eV and 951.2 eV, corresponding to Cu-2p3/2 and Cu-2p1/2 of metallic Cu, respectively, suggesting that metallic Cu is present on the surface of STO nanoparticles. It should be noted that the content of Pt is very low (~5 mol%) in the alloy, the XPS peak position are very close to those of pure Cu, which is in good agreement with XRD results. Furthermore, in the XPS spectrum illustrated in Fig. 2C, the peaks appeared at binding energy (BE) of 70.4 eV and 73.7 eV, which is identical to metallic Pt (4f7/2, 70.4 eV) and Pt (4f5/2, 73.7 eV).[25] This implies that the loaded Pt exists in the metallic form Pt(0) in the sample. Thus, the XPS analysis further verified that this preparation process of STO/Cu95-Pt5 sample could resist oxidization.

Moreover, the morphologies of pure STO and the STO nanoparticles loaded with Cu-Pt alloy were characterized with TEM images, as shown in Fig. 3. Clearly, the bimetallic Cu-Pt nanoparticles are homogeneously loaded on the surface of STO particles (Fig. 3B), and their average size is measured to be about 3 nm. Also, this sample of STO/Cu95-Pt5 exhibits similar morphology to the bare STO nanoparticles (Fig. 3A), indicating that the introduction of bimetallic Cu-Pt alloy does not obviously change the morphology of STO nanoparticles. High-resolution TEM images showed that the Cu-Pt nanoparticles were attached onto the highly crystallized STO surfaces (Fig. 3C). The visible lattice fringes of 0.21 nm can be ascribed to the expected d-spacing of the (111) plane of the Cu-Pt alloy.[17] Also, the obvious lattice fringes of 0.225 nm assigned to (111) crystalline planes of cubic STO.[26] Moreover, no lattice fringes according to pure Cu or pure Pt were observed on a large scale, demonstrating the alloying nature of the Cu-Pt nanoparticles.[27,28]

Based on above results, the components of the as-synthesized sample could be defined as Cu, Pt and STO, and the Cu-Pt alloy nanoparticles are homogeneously loaded on the STO surface. And, the close interconnection between Cu-Pt alloy and STO would be favorable for the transfer of photogenerated electrons from Cu-Pt to STO nanoparticles, thus enhancing the charge separation and photocatalytic hydrogen generation efficiency.

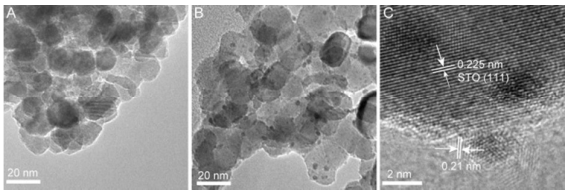

Fig. 3 TEM images of pure STO (A), STO/Cu95-Pt5 (B), and high-resolution TEM image of STO/Cu95-Pt5 (C).

As shown in Fig. 4, the photocatalytic hydrogen production activities of pure STO and STO/Cu-Pt were evaluated under high-pressure mercury lamp irradiation using methanol as a scavenger. It can be seen that pure STO shows a very low photocatalytic activity because of the rapid recombination of conduction band (CB) electrons and valence band (VB) holes. Surprisingly, the introduction of the Cu-Pt alloy cocatalyst results in a significant improvement in the photocatalytic hydrogen production activity of STO, and the content of Cu and Pt in the cocatalyst has a significant

influence on the photocatalytic activity. The photocatalyst with only Cu cocatalyst (STO/Cu100-Pt0) shows decent photocatalytic activity with a hydrogen production rate of 132.3 μmol·h^{-1}, because the nano-sized Cu could help in the charge separation and act as a reaction site for water reduction, thereby enhancing the photocatalytic hydrogen production activity of STO nanoparticles. Here, if a spot of Pt is introduced in the cocatalyst, the activity of the sample can be obviously enhanced. Obviously, when the Pt content reaches 5.0% (STO/Cu95-Pt5), the highest hydrogen production rate is up to 369.4 μmol·h^{-1}, and the rate exceeded that obtained on pure STO and STO/Cu100-Pt0 by more than 46.6 and 2.79 times, respectively. Furthermore, the increase in the Pt content in the cocatalyst (Cu90-Pt10, Cu10-Pt90 and Cu0-Pt100) leds to a gradual reduction of the photocatalytic hydrogen production activity. Also, the apparent quantum yields of hydrogen production for STO/Cu95-Pt5 increased by 64.54% than STO/Cu0-Pt100,[29] further verified that STO/Cu95-Pt5 photocatalyst with high photocatalytic activity for hydrogen generation. Therefore, the synergetic effect between Cu and Pt in the cocatalyst could more efficiently accept and transport electrons from the excited semiconductor, suppress charge recombination, improve interfacial charge transfer processes, which makes the Cu-Pt alloy become a more efficient cocatalyst.

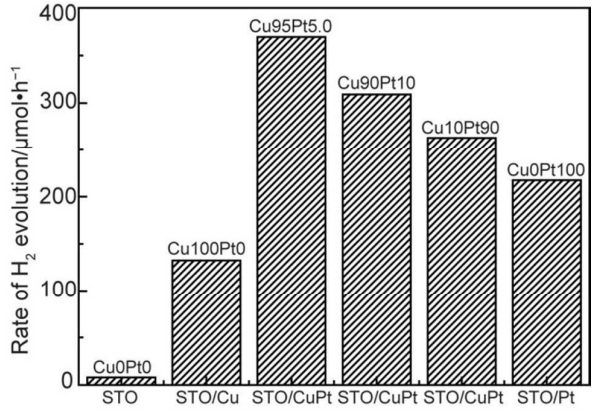

Fig. 4 Photocatalytic hydrogen evolution over the STO nanoparticles loaded with Cu-Pt alloy.

As mentioned above, the STO nanoparticles loaded with bimetallic Cu-Pt alloy was prepared using a photo-deposition method. Thus, we speculate that the loading route of Cu-Pt alloy would have obvious effect on the photocatalytic activity of STO nanoparticles for hydrogen evolution. As shown in Fig. 5, clearly, the simultaneous loading of Cu and Pt on the STO nanoparticles exhibits the highest hydrogen production rate after irradiated for 30 min by high-pressure mercury lamp (Fig. 5a). When the Cu and Pt source are successively added into the aqueous methanol suspension of STO nanoparticles (Fig. 5b), and also irradiated for 30 min, the photocatalytic activities of samples gradually reduce for hydrogen production. Similarly, the successive loading of Pt and Cu also results in a significant reduction on the photocatalytic activity of the STO nanoparticles (Fig. 5c). Therefore, these results further verified that the synergetic effect between the Cu and Pt component would originate from the alloying of Cu and Pt.

Also, the stability of STO/Cu95-Pt5 is investigated. As shown in Fig. 6, the rate of hydrogen generation is the maximum (365 μmol·h^{-1}) in the first run, and then declines slightly in the consecutive runs. After consecutive 4 runs, clearly, the rate of hydrogen generation could still reach 275 μmol·h^{-1}. The recycling experiment shows that STO/Cu95-Pt5 does not exhibit any significant loss of activity, indicating that the bimetallic cocatalysts are stable during the photocatalytic hydrogen production. In contrast, STO/Cu100-Pt0 shows an unstable catalytic performance, and the amount of hydrogen evolution after 4 runs (87.5 μmol·h^{-1}) is only half of the rate in the first run (175 μmol·h^{-1}). Thus, the synergetic effect between Pt and Cu in the cocatalyst resulted in a significant enhancement of the photocatalytic activity, improved the chemical stability and prolonged the lifetime of the photocatalyst.

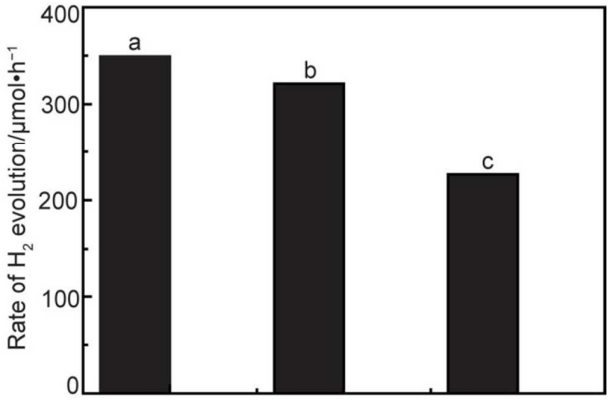

Fig. 5 The loading route effect on the photocatalytic hydrogen evolution activity of the STO nanoparticles loaded with Pt and Cu, (a) the simultaneous loading of Cu and Pt on the STO nanoparticles, (b) the successive loading of Cu and Pt on the STO nanoparticles, (c) the successive loading of Pt and Cu on the STO nanoparticles (total amount of Cu and Pt 1.5 mol%, the content of Cu 95%, the content of Pt 5%).

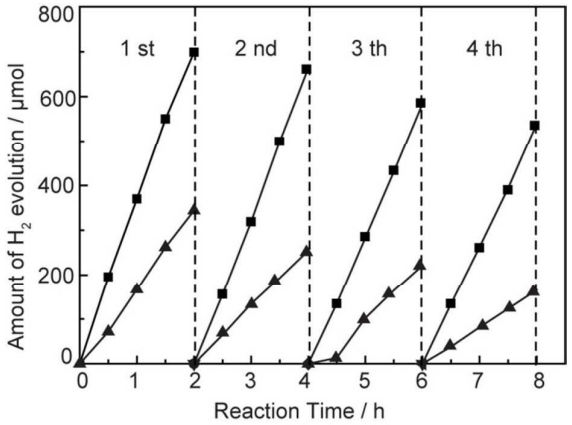

Fig. 6 Cyclic hydrogen evolution curves over STO/Cu95-Pt5 (■) and STO/Cu100-Pt0 (▲).

In order to demonstrate that the bimetallic Cu-Pt alloy could effectively accept the photoexcited charge carriers from the STO

nanoparticles, the photoluminescence (PL) quenching experiments were employed. As shown in Fig. 7, clearly, more effective PL quenching of STO/Cu95-Pt5 is observed (Fig.7c) in comparison with STO/Cu100-Pt0 (Fig.7b), because the electrons excited from the CB of the semiconductor are injected more easily into the bimetallic Cu-Pt alloy. The effective charge carrier separation will prolong the reactive electron and hole lifetimes and increase the photocatalytic activity of the photocatalysts. However, the characteristic emission peaks of STO are almost disappeared when Pt is loaded on the STO nanoparticles, which is not in good agreement with the above results. It is well known that copper requires a high overpotential of ca. 250–300 mV for hydrogen generation,[30–33] and Pt possesses high hydrogen evolution reaction activity with nearly zero overpotential.[34-36] Thus, the possible explanation is that the introduction of Cu-Pt alloy will cause decreasing of the overpotential of hydrogen evolution. As a result, the high photocatalytic activity may be ascribed to two causes, i. e. more efficient separation of electron-hole pair and lower overpotential of hydrogen evolution.

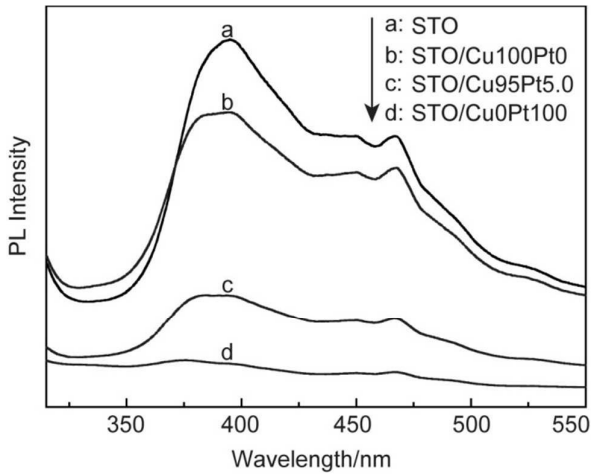

Fig. 7 Photoluminescence (PL) spectra of pure STO (a), STO/Cu100-Pt0 (b), STO/Cu95-Pt5 (c) and STO/Cu0-Pt100 (d), λ_{ex} = 339 nm.

4 Conclusion

In summary, the proposed simple photo-reduction synthesis of the STO nanoparticles loaded with Cu-Pt alloy afforded an effective photocatalyst for hydrogen production. STO/Cu95-Pt5 shows the highest photocatalytic hydrogen production activity with a rate as high as 369.4 $\mu mol \cdot h^{-1}$. It is believed that the high photocatalytic activity may be ascribed to the positive synergetic effect between Cu and Pt, which could more efficiently suppress charge recombination and improve interfacial charge transfer. This study shows that the development of titania-based photocatalyst containing an inexpensive and highly activity Cu-Pt cocatalyst is feasible and has a great potential for photocatalytic hydrogen production.

Acknowledgements

This work was financially supported by the National Natural Science Foundation of China (Grant No. 21305092, 21301118), and the Shanghai Municipal Natural Science Foundation (No. 13ZR1461800).

Notes and references

1 M. Ni, M. K. H. Leung, D. Y. C. Leung and K. Sumathy, *Renew. Sust. Energ. Rev.* 2007, **11**, 401–425.
2 Y. Guo, S. Z. Wang, D. H. Xu, Y. M. Gong, H. H. Ma and X. Y. Tang, *Renew. Sust. Energ. Rev.* 2010, **14**, 334–343.
3 A. Fujishima and K. Honda, *Nature*, 1972, **238**, 37–38.
4 A. Kudo and Y. Miseki, *Chem. Soc. Rev.* 2009, **38**, 253–278.
5 K. Maeda, A. Xiong, T. Yoshinaga, T. Ikeda, N. Sakamoto, T. Hisatomi, M. Takashima, D. Lu, M. Kanehara, T. Setoyama, T. Teranishi and K. Domen, *Angew. Chem. Int. Ed.* 2010, **122**, 4190–4193.
6 J. Zhang, J. Yu, Y. Zhang, Q. Li and J. R. Gong, *Nano Lett*. 2011, **11**, 4774–4779.
7 R. Asai, H. Nemoto, Q. Jia, K. Saito, A. Iwasea and A. Kudo, *Chem. Commun*. 2014, **50**, 2543–2546.
8 P. Reunchan, S. Ouyang, N. Umezawa, H. Xu, Y. Zhang and J. Ye, *J. Mater. Chem. A*. 2013, **1**, 4221–4227.
9 T. K. Townsend, N. D. Browninga and F. E. Osterloh, *Energy Environ. Sci.* 2012, **5**, 9543–9550.
10 L. Yang, H. Zhou, T. Fan and D. Zhang, *Phys. Chem. Chem. Phys.* 2014, 16, 6810–6826.
11 J. Shi, *Chem. Rev*. 2013, **113**, 2139–2181
12 H. L. Jiang and Q. Xu, *J. Mater. Chem*. 2011, **21**, 13705–13725.
13 X. Zhang and Z. Su, *Adv. Mater*. 2012, **24**, 4574–4577.
14 S. Tang, S. Vongehr and X. Meng, *J. Mater. Chem*. 2010, **20**, 5436–5445.
15 H. L. Jiang, T. Akita, T. Ishida, M. Haruta and Q. Xu, *J. Am. Chem. Soc.* 2011, **133**, 1304–1306.
16 C. H. Liu, X. Q. Chen, Y. F. Hu, T. K. Sham, Q. J. Sun, J. B. Chang, X. Gao, X. H. Sun and S. D. Wang, *ACS Appl. Mater. Interfaces* 2013, **5**, 5072–5079.
17 X. Cao, N. Wang, S. Jia and Y. Shao, *Anal. Chem*. 2013, **85**, 5040–5046.
18 H. Xie, J. Y. Howe, V. Schwartz, J. R. Monnier, C. T. Williams and H. J. Ploehn. *J. Catal.* 2008, **259**, 111–122.
19 L. C. Li, C. S. Wang, X. X. Ma, Z. H. Yang, X. H Lu, *Chinese J. Catal*. 2012, **33**, 1778–1782.
20 X. X. Han, Q. Chen and R. X. Zhou, *J. Mol. Catal. A-Chem*. 2007, **277**, 210–214.
21 Q. Yao, Z. H. Lu, Y. Wang, X. Chen and G. Feng, *J. Phys. Chem. C*. 2015, **119**, 14167–14174.
22 Y. Shiraishi, H. Sakamoto, Y. Sugano, S. Ichikawa and T. Hirai, *ACS NANO*, 2013, **7**, 9287–9297.
23 S. Chen, H. Zhang, L. Wu, Y. Zhao, C. Huang, M. Ge and Z. Liu, *J. Mater. Chem*. 2012, **22**, 9117–9122.
24 H. Kato, M. Kobayashi, M. Hara and M. Kakihana, *Catal. Sci. Technol*. 2013, 3, 1733–1738.
25 J. Croy, S. Mostafa, J. Liu, Y. H. Sohn and C. B. Roldan. *Catal. Lett*. 2007, **118**, 1–7.
26 X. Yue, J. Zhang, F. Yan, X. Wang and F. Huang, *Appl. Surf. Sci.* 2014, **319**, 68–74
27 Y. Ding, Y. Wang, L. C. Zhang, H. Zhang and Y. Lei, *J. Mater. Chem.* 2012, **22**, 980–986.
28 C. X. Xu, Y. Q. Liu, F. Su, A. H. Liu and H. J. Qiu, *Biosens. Bioelectron*. 2011, **27**, 160–166.
29 S. R. Kadam, D. J. Late, R. P. Panmand, M. V. Kulkarni, L. K. Nikam, S. W. Gosavi, C. J. Park and B. B. Kale, *J. Mater. Chem. A*, 2015, **3**, 21233–21243.
30 W. Sheng, M. Myint, J. G. Chen and Y. Yan, *Energy Environ. Sci.* 2013, **6**, 1509–1512.

31 B. Kumar, S. Saha, A. Ganguly and A. K. Ganguli, *RSC Adv.* 2014, **4**, 12043–12049.
32 B. Kumar, S. Saha, M. Basu and A. K. Ganguli, *J. Mater. Chem. A* 2013, **1**, 4728–4735.
33 B. Kumar, S. Saha, K. Ojha and A. K. Ganguli, *Mater. Res. Bull.* 2015, **64**, 283–287.
34 Y. Li, H. Wang, L. Xie, Y. Liang, G. Hong and H. Dai, *J. Am. Chem. Soc.* 2011, **133**, 7296-7299.
35 M. A. Lukowski, A. S. Daniel, F. Meng, A. Forticaux, L. Li and S. Jin, *J. Am. Chem. Soc.* 2013, **135**, 10274-10277.
36 B. Winther-Jensen, K. Fraser, C. Ong, M. Forsyth and D. R. MacFarlane, *Adv. Mater.* 2010, **22**, 1727-1730.

Synergetic effect of Cu-Pt bimetallic cocatalyst on $SrTiO_3$ for efficient photocatalytic hydrogen production from water

Lixia Qin,[a] Guofeng Si,[a] Xiangqing Li,[a] Shi-Zhao Kang*[a]

[a]*School of Chemical and Environmental Engineering, Shanghai Institute of Technology, 100 Haiquan Road, Shanghai 201418, China*

* To whom correspondence should be addressed. E-mail: kangsz@sit.edu.cn.

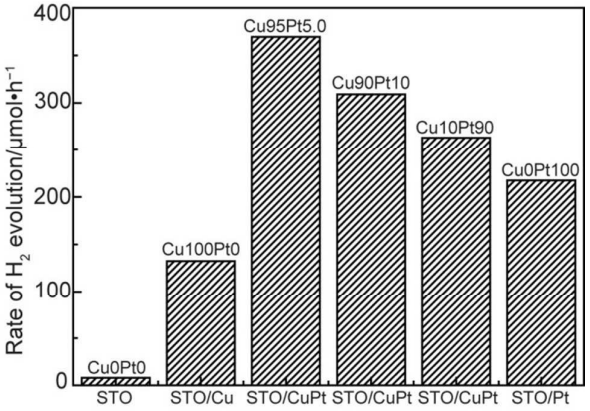

The introduction of the Cu-Pt bimetal as cocatalyst results in a significant improvement in the photocatalytic hydrogen production activity of STO. Surprisingly, the hydrogen generation efficiency over the STO/Cu95-Pt5 photocatalyst was about 46.6 and 2.79 times of STO and STO/Cu100-Pt0, respectively.